nature communications

Article

https://doi.org/10.1038/s41467-026-71825-x

Trees halve urban heat island effect globally but unequal benefits only modestly mitigate climate-change warming

Received: 26 June 2025

Accepted: 24 March 2026

Published online: 06 May 2026

Check for updates

Robert I. McDonald[1,2,3] ✉, TC Chakraborty[4] ✉, Theodore A. Endreny[5], Luke A. Parsons[6], Mariami Marsagishvili[1] & Manuel Esperon-Rodriguez[7,8]

Although tree cover reduces the urban heat island, no global estimate quantifies air temperature reductions by contemporary or future tree cover, currently and with climate change. Here, we estimate these reductions for all 8,919 large urban areas. Current urban tree cover mitigates 41–49% of the maximum potential air-temperature urban heat island that would occur in the absence of tree canopy. Tree canopy reduces summer air temperature by a population-weighted mean of 0.15 ± 0.03 °C, with wide variation (0.0–2.7 °C), benefiting 914 (805–1040, 95% CI) million people by >0.25 °C. Cooling benefits are greater in already cooler areas: high-income countries and suburbs. Current and plausible future tree cover mitigate only ~10% (6.7–18% and 6.3–17%, respectively) of the median mid-century climate-change warming under a moderate emission scenario. Our results suggest tree canopy expansion in densely settled low-income urban areas is necessary for equitable urban heat island mitigation and climate adaptation.

Heat and high air temperatures (AT) are a significant public health threat, killing an estimated 356,000 people globally in 2019, with the most intense impacts in South and Southeast Asia, Africa, and the Middle East[1]. These challenges are exacerbated in urban areas, where the urban heat island (UHI) effect can significantly increase AT compared to the AT in surrounding rural areas[2–4]. The UHI effect happens because cities contain large amounts of surfaces like concrete and asphalt, which absorb energy from incoming solar radiation and later emit it as thermal radiation[5]. The surface geometry of buildings and roads can be important in determining which surfaces receive solar insolation and hence heat up, as can factors such as latitude and sun angle[6]. The UHI intensity is often measured by comparing temperatures, either land surface temperature (LST) or AT, in city centers with those in surrounding rural areas[7]. UHI globally averages above 1.0 °C for LST and slightly <0.5 °C for AT[8] during daytime, although estimates depend on the spatial resolution of sensors used[8], the algorithm for selecting background areas[8], and whether averages are population-weighted within or across cities[9]. The UHI can be reduced by shading built-up surfaces or by increasing their albedo, thus reducing the absorption of solar energy, or by increasing evapotranspiration, which enhances evaporative dissipation of heat[10].

Future climate change will substantially increase heat stress globally, and thus the impact of extreme heat on human health[11]. Historical climate change has already increased global average AT by around 1.1 °C, and future warming is projected to reach 1.5 °C between 2030 and 2035[12]. Beyond average AT, climate change is also expected to make heat waves more frequent[13]. Already, the average frequency of heat waves per year has increased from two per year in 1971 to four per year in 2022[14]. Heat waves are also projected to get more intense, and the Northern Hemisphere summer of 2023 was the warmest of the past 2000 years[15]. According to the Intergovernmental Panel on Climate Change (IPCC), life-threatening heat is expected to impact between

[1]The Nature Conservancy in Europe, Berlin, Germany. [2]CUNY Institute for Demographic Research, City University of New York, New York, NY, USA. [3]Geography Department, Humboldt University, Berlin, Germany. [4]Atmospheric Sciences and Global Change Division, Pacific Northwest National Laboratory (PNNL), Richland, WA, USA. [5]Department of Environmental Resources Engineering, SUNY College of Environmental Science and Forestry (ESF), Syracuse, NY, USA. [6]Global Science, The Nature Conservancy, Salt Lake City, UT, USA. [7]Hawkesbury Institute for the Environment, Western Sydney University, Penrith, NSW, Australia. [8]School of Science, Western Sydney University, Penrith, NSW, Australia. ✉e-mail: rob_mcdonald@tnc.org; tirthankar.chakraborty@pnnl.gov

half and three-fourths of the global population by 2100[13]. These changes are projected to increase annual heat-related mortality by 3.0–12.7% points, depending on the region and the greenhouse gas emissions scenario used, if additional adaptation measures are not taken[16].

Cities thus face a dual heat challenge, of mitigating the UHI while preparing for additional warming from climate change. Many cities are engaging in heat action planning and designing programs that reduce residents' exposure and vulnerability to extreme heat[17,18]. One part of heat action planning is reducing exposure to excessive outdoor temperatures, which is often accomplished by increasing tree canopy cover[9]. Trees cool the environment via evapotranspiration[19], which increases evaporative dissipation of heat[20], and via shading, which reduces solar radiation hitting and being absorbed by surfaces such as asphalt and concrete. Taken together, these two phenomena reduce AT on average by 1–2 °C directly under a row of street trees, according to a review of studies using field measurements of the cooling effect of street trees[19]. Trees reduce AT within a few hundred meters of the tree canopy, although this distance varies with factors such as the size of the canopy patch[21], wind speed, and relative humidity[9]. These cooling benefits in aggregate can be quite significant. Tree cover in 2016 in the United States (US), for instance, was estimated to save around 1200 lives per year that would otherwise be lost due to excess heat[4].

Research on urban heat risk and tree cover shows that both are unequally distributed[9,22]. Globally, cities in lower-income countries generally have higher population exposure to heat stress than higher-income countries, partly because lower-income countries tend to be in hotter climates[23]. Cities in lower-income regions also tend to have lower tree canopy cover than cities in higher-income regions[24] due to differences in urban form and cultural preferences, resources available for tree planting and maintenance, and climate[9]. This inequality in heat risk and tree cover also occurs within urban areas. For instance, one survey of US cities found that in 92% of communities, low-income neighborhoods were often located in city centers, had on average 15% less tree cover, and were 1.5 °C LST hotter than high-income neighborhoods, which were often more suburban[25]. Multiple other studies show similar results using different methodologies, consistently finding that in most US cities, lower-income and minority populations live in neighborhoods with higher summer LST[26,27], and similar patterns have been observed in some other countries[28–30], although there are exceptions depending on the country[31] and scale of analysis[32].

Despite the critical cooling benefits trees provide for all urban areas, there are several gaps in current global knowledge. First, many global studies that have quantified the UHI have focused on LST[33,34], although there are studies quantifying AT[35–37]. Similarly, many multi-city studies of tree cooling used satellite-derived LST alone[38–40], which is not appropriate for quantifying heat risk to human health[36,41], rather than AT or other metrics more related to human health. There are, however, exceptions, such as Ibsen et al.'s analysis of eight US cities[42] and Du et al.'s analysis of AT cooling for 392 European urban clusters[36]. The magnitude and global geography of tree cooling of AT has not been directly compared with global patterns of the AT UHI, although there are local and regional studies that have looked at specific cities[43,44].

Second, spatially explicit climate change projections of urban temperature increase are rarely compared with estimates of current or plausible future tree cooling, and increasing knowledge around how to plan for urban tree canopy given a rapidly changing climate was called out as a knowledge gap in a recent review paper[45].

Third, there are only a few global multi-city studies and reviews of the AT cooling benefits trees provide, such as Li et al.'s meta-analysis of 110 cities/regions[46] and Su et al.'s analysis of 35 cities[47]. There are no global assessments of AT cooling for all major urban areas using a consistent methodological approach, limiting the study of the distribution and equity of tree cooling benefits relative to climate, income, and urban form[48].

Here, we conduct a comprehensive global assessment of AT cooling benefits using a statistical model. Our analysis looks at all 8919 large urban areas globally, which captures the full range of climatic, geographic, and socioeconomic contexts where urban populations reside. Our analysis workflow is shown in Fig. 1. We assembled remotely sensed information for all large functional urban areas[49] (FUAs) globally, including measurements of tree canopy cover and LST, as well as gridded urban-resolving estimates of AT. Input datasets were used to fit a hierarchical statistical model that predicts the local AT anomaly given local tree canopy and other land cover, with parameters varying by climate zone and geographic position. We also supplemented this global analysis with simulations using a process-based model for three case study cities that span a climatic gradient from arid to humid, which allows us to capture the impact of urban trees on a more complete heat stress metric, namely the wet bulb globe temperature (WBGT), Finally, we estimated for all large cities the magnitude of the UHI and increases in summer AT due to climate change. The magnitudes of these quantities were then compared with output from our statistical and process models. Our analysis answers three research questions: How much bigger would the AT UHI be on average without urban tree canopy? How much is AT cooling from the current or plausible future urban tree canopy able to mitigate AT warming due to climate change? How equally are AT cooling benefits distributed with respect to climate, level of economic development, and population density?

Results

Urban tree canopy and UHI mitigation

Overall, urban tree cover counteracts just under half of the maximum potential UHI (Fig. 2). The maximum potential UHI is the estimated difference between urban air temperatures and those in rural reference areas that would be observed without any tree cover, and averages 0.31 ± 0.01 °C globally. With tree cover, the observed AT UHI on average is estimated at 0.16 ± 0.1 °C globally with the simplified urban extent (SUE) algorithm, which defines rural reference as the non-urban non-water pixels within each FUA. That is, urban tree cover currently mitigates 48.6 ± 1.3% of the maximum potential AT UHI for FUAs around the globe. For comparison, the observed AT UHI with the buffering algorithm, which defines pixels in a buffer area outside each FUA as the rural reference, is 0.22 ± 0.1 °C, so with that higher estimate of observed UHI, urban tree cover mitigates only 41.3 ± 1.3% of the maximum potential AT UHI. Note that both the maximum potential UHI and the observed UHI vary with latitude (Supplementary Fig. 1) and are, on average, greater at higher latitudes than at lower latitudes.

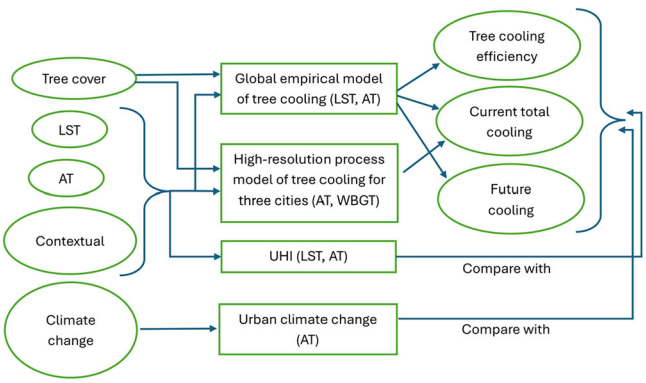

Fig. 1 | Analysis workflow of the stages of our analysis. Input data (left column) were used in a series of models (middle column) to estimate three principal factors (right column). LST land surface temperature, AT air temperature, UHI urban heat island, WBGT wet bulb globe temperature.

https://doi.org/10.1038/s41467-026-71825-x

Urban tree canopy and climate change adaptation

Global average population-weighted urban tree cover is 18.3 ± 0.3%. We evaluated three additional global scenarios of tree cover: (1) a 10% increase in tree cover in each 1 km cell, used to quantify tree cooling efficiency; (2) complete loss of existing tree canopy, used to estimate the total cooling currently provided by trees; and (3) a maximum plausible increase in tree canopy, given constraints of climate and urban form. We estimate that without any urban tree cover, under our total tree cover loss scenario, the population-weighted urban AT would be 0.151 ± 0.003 °C higher. Under the maximum plausible increase scenario, global average tree cover increases to 32.8 ± 0.4%. At this greater extent of urban tree cover, total population-weighted urban AT would be 0.295 ± 0.003 °C lower.

In order to compare current and potential future tree cooling benefits against climate change impacts, we assessed summer warming projections from SSP2–4.5, a "middle of the road" GHG emissions scenario that, of the SSPs, most closely aligns with pledged reductions in emissions under the Paris Accords[50]. Specifically, we examine projections of daytime summer AT change for the 20-year period centered around the year 2050, calculating the multi-model median, 5th, and 95th percentiles based on NASA NEX GDDP downscaled CMIP6 models (constraining the ensemble to those models showing warming in the range of 'likely' equilibrium climate sensitivity (ECS))[51]. For the world's FUAs, the median projected temperature increase is on average 1.5 °C (0.86–2.3 °C for the 5th and 95th percentiles of the ensemble) (Fig. 2). In comparison, the current tree cover only cools 10% (6.7–18%) of this value. Under our maximum plausible future tree planting scenario, the additional tree cover would cool air temperatures by an additional 0.14± 0.2 °C. In other words, under the maximum plausible future tree planting scenario, total cooling benefits by trees would be only 20% (13–35%) of the projected temperature increase with climate change.

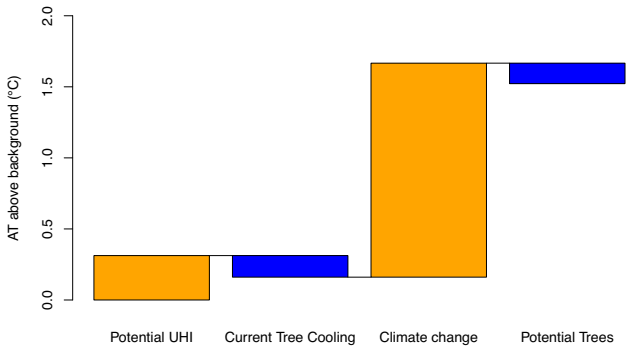

Fig. 2 | Average air temperature (AT) changes due to several factors. Shown are an estimate of the maximum potential urban heat island (UHI) using the simplified urban extent (SUE) algorithm; the current average cooling effect of tree cover; the projected ensemble median (CMIP6 and SSP2–4.5) increase in summer temperature by 2050 due to climate change; and the average cooling effect of potential new tree cover under the maximum feasible planting scenario. See text for discussion of uncertainty.

Tree canopy cover distribution

Globally, urban tree cover declines on average with increasing population density (Fig. 3), with low-density suburbs and exurbs having twice the tree cover of more densely populated urban centers. By contrast, impervious cover increases with increasing population density, from <20% in low-density suburbs and exurbs to almost 80% in high-density urban centers. Most of the area in FUAs (94%) has relatively low population density (<5000 people/km^2), so much of the land surface has relatively high tree cover and low impervious cover. However, most people in FUAs (54%) live in the remaining densely

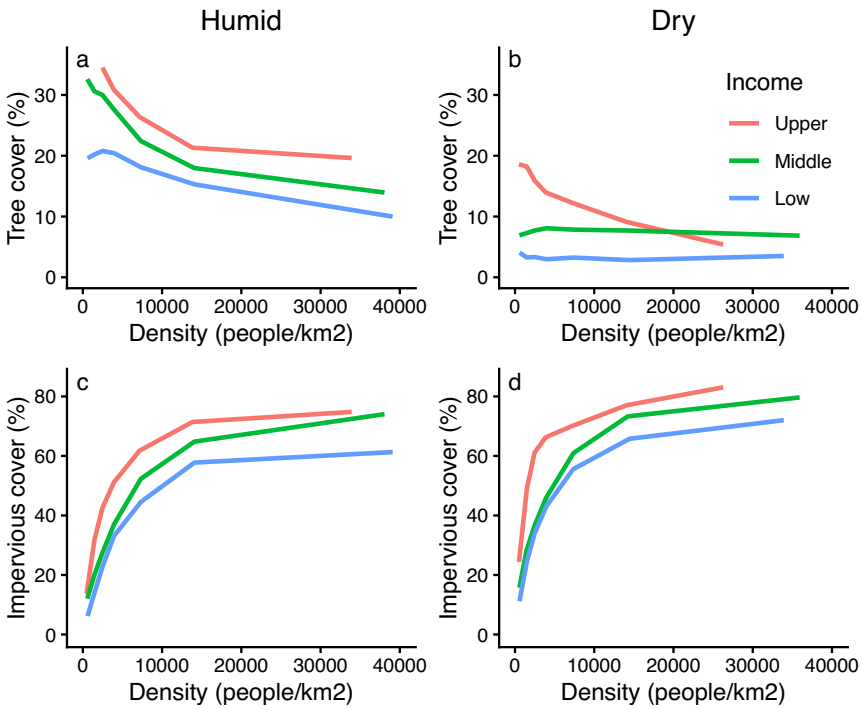

Fig. 3 | Average population-weighted tree canopy cover (top row) and impervious surface cover (bottom row) as a function of population density, by country-level income category (upper income, middle income, or low-income) and aridity. a Tree cover for FUAs in humid climates. **b** Tree cover for FUAs in dry climates. **c** Impervious cover for FUAs in humid climates. **d** Impervious cover for FUAs in dry climates. Humid climates (AI > 0.5) are shown in the left column, while dry arid or semi-arid climates (defined as an Aridity Index, AI < 0.5) are shown in the right column. Displayed is the average tree canopy and impervious surface cover for categories of population density.

https://doi.org/10.1038/s41467-026-71825-x

Table 1 | Estimated average population-weighted tree cooling efficiency (TCE) as a function of impervious surface cover in the neighborhood by climate zone

LST reduction (°C)	Impervious cover			
Aridity category	**0–25%**	**25–50%**	**50–75%**	**75–100%**
Arid	0.95 ± 0.031	0.94 ± 0.031	0.90 ± 0.032	0.85 ± 0.032
Semi-Arid	0.56 ± 0.012	0.60 ± 0.012	0.62 ± 0.012	0.64 ± 0.013
Dry subhumid	0.51 ± 0.014	0.61 ± 0.013	0.67 ± 0.014	0.73 ± 0.015
Humid	0.42 ± 0.006	0.62 ± 0.006	0.73 ± 0.007	0.82 ± 0.007
AT reduction (°C)	**Impervious cover**			
Aridity category	**0–25%**	**25–50%**	**50–75%**	**75–100%**
Arid	0.27 ± 0.008	0.27 ± 0.008	0.26 ± 0.008	0.25 ± 0.008
Semi-Arid	0.12 ± 0.003	0.13 ± 0.003	0.13 ± 0.003	0.14 ± 0.003
Dry subhumid	0.09 ± 0.003	0.10 ± 0.003	0.11 ± 0.003	0.12 ± 0.004
Humid	0.08 ± 0.001	0.09 ± 0.002	0.10 ± 0.002	0.12 ± 0.002

TCE is defined as the change in land surface temperature (LST) or air temperature (AT) in °C for a 10% increase in tree cover, and accounts for land use nearby. The error range shown is the standard error of the TCE, as calculated from the regression coefficients.

populated 6% of FUAs (that is, areas >5000 people/km^2). The population-weighted average density (that is, the average population density experienced by urban residents; see Methods for details) is 5643 ± 47 people/km^2, so the typical urban resident lives in a neighborhood with relatively less tree cover (18.1 ± 0.2%) and relatively more impervious cover (39.0 ± 0.2%) than would be found in more sparsely settled portions of the FUA.

The average gradient between tree cover and population density is modulated by other factors. In FUAs in humid climates, the average tree cover is higher, and there is a strong gradient between tree cover and population density. Conversely, in FUAs with a dry climate, there is less tree cover and no clear gradient between tree cover and density, except for those in high-income countries. Across climates, higher-income countries have greater tree cover. Note, however, that the aridity index (AI) class is correlated with income (Supplementary Fig. 2), with almost half (46%) of urban dwellers in large FUAs in low-income countries being in arid or semi-arid climates, compared with 21% of urban dwellers in large FUAs in high-income countries. Impervious cover is also greater in high-income countries than in low-income countries.

Variation in tree cooling efficiency

One way to estimate the effect of trees on temperature is the tree cooling efficiency (TCE), defined here as the change in AT for a 10% increase in tree cover (Table 1). We find that TCE is greater for LST than AT by a factor of four. AT TCE is also greater in more arid climates than in more humid ones. Finally, TCE varies with the amount of impervious cover in the neighborhood (Table 1). For most climates, greater amounts of impervious cover are associated with greater TCE. This occurs because in neighborhoods with high impervious cover, the incremental addition of 10% more tree cover displaces impervious surface cover, rather than other land cover types like sparse vegetation (e.g., lawns). This gradient between TCE and the amount of impervious cover is strongest in humid climates and less strong in the dry subhumid and semi-arid climates. In arid climates, more impervious cover is not associated with a meaningful change in the AT TCE and a small decrease in LST TCE.

Distribution of tree cooling benefits

Another way to estimate the effect of trees on temperature is the total cooling, defined as the estimated reduction in summer daytime AT compared with a baseline case of no tree cover. The total cooling varies widely among FUAs (Fig. 4). Total cooling is the greatest in North America and Europe, where countries have more humid climates and higher incomes, both leading to greater tree canopy cover. Conversely, total cooling is least in arid parts of lower-income countries (Fig. 3). Variation among FUAs in total cooling is high, from 0 to 1.3 °C. Variation at the 1 km scale is even higher, ranging from 0 to 2.7 °C.

Within FUA, the total cooling by trees follows a predictable pattern relative to the amount of impervious land cover (Fig. 4b). More impervious cover is associated with a greater observed UHI. With no tree cover, the maximum potential UHI would be realized, which would reach its peak in urban centers with elevated levels of impervious cover. The total cooling (i.e., potential minus observed UHI) is greater in areas of less impervious cover, simply because there is more tree cover in those locations (Fig. 3). In a sense, total cooling is greater where AT is already relatively low, in suburban and exurban areas with low UHI.

Spatial patterns from the New York City FUA illustrate this trend (Fig. 4c). The magnitude of total cooling is highest in outlying areas, like suburban areas of Bridgeport and Tom's River, decreases in peripheral towns like Edison, and is smallest in the dense cover of New York City proper. TCE in humid climates is the highest in dense, impervious neighborhoods, but these same areas exhibit smaller total cooling due to lower canopy cover. Within the New York City FUA, population-weighted average total cooling is 0.26 °C, with an observed range of 0–0.68 °C.

Distribution of current and future cooling benefits

People in FUAs in higher-income countries receive more total cooling. Upper-income countries have a population-weighted average cooling of 0.23 ± 0.03 °C, while middle-income countries have an average cooling of 0.15 ± 0.03 °C, and low-income countries have an average cooling of 0.08 ± 0.03 °C. However, some people receive far more AT reduction (Fig. 5). In upper-income countries, 40% (35–44%, 95% CI) of people receive an AT reduction of 0.25 °C or greater, and 7.7% (6.3–9.4%) of people receive an AT reduction of at least 0.5 °C. By contrast, in low-income countries, 8.9% (7.2–10.7%) of people receive an AT reduction of 0.25 °C or greater, and 1.1% (0.9–1.3%) of people receive an AT reduction of at least 0.5 °C. Across all income categories, globally 914 (805–1040) million people receive an AT reduction of 0.25 °C or greater, and 203 (169–243) million people receive an AT reduction of at least 0.5 °C.

Under the maximum plausible increase scenario, low-income countries would have a large increase in AT reduction benefits (i.e., temperature decreases experienced by residents) over current levels, with tree cover under this scenario (i.e., current plus plausible future additional tree cover) providing 66% (57–71%) of people an AT reduction of 0.25 °C or greater, and 6.0% (2.5–12%) of people an AT reduction of at least 0.5 °C. Even upper-income countries, however, could have a significant increase in AT reduction benefits, with tree cover under this scenario providing 67% (60–74%) of people an AT reduction of 0.25 °C or greater and 10% (7.7–15%) of people an AT reduction of at least 0.5 °C.

Patterns of total cooling at the country-level are a complex function of climate, economic development, and patterns of urbanization (Supplementary Fig. 3). There is a set of high-income countries in humid climates that have prominent levels of total cooling, such as the United States, France, and Japan. Middle-income countries that are, on average, in humid climates like China and Brazil have modest levels of total cooling. Countries in semi-arid or arid climates (e.g., Mexico and Saudi Arabia) or countries with low income (e.g., the Democratic Republic of Congo) have the lowest levels of total cooling.

https://doi.org/10.1038/s41467-026-71825-x

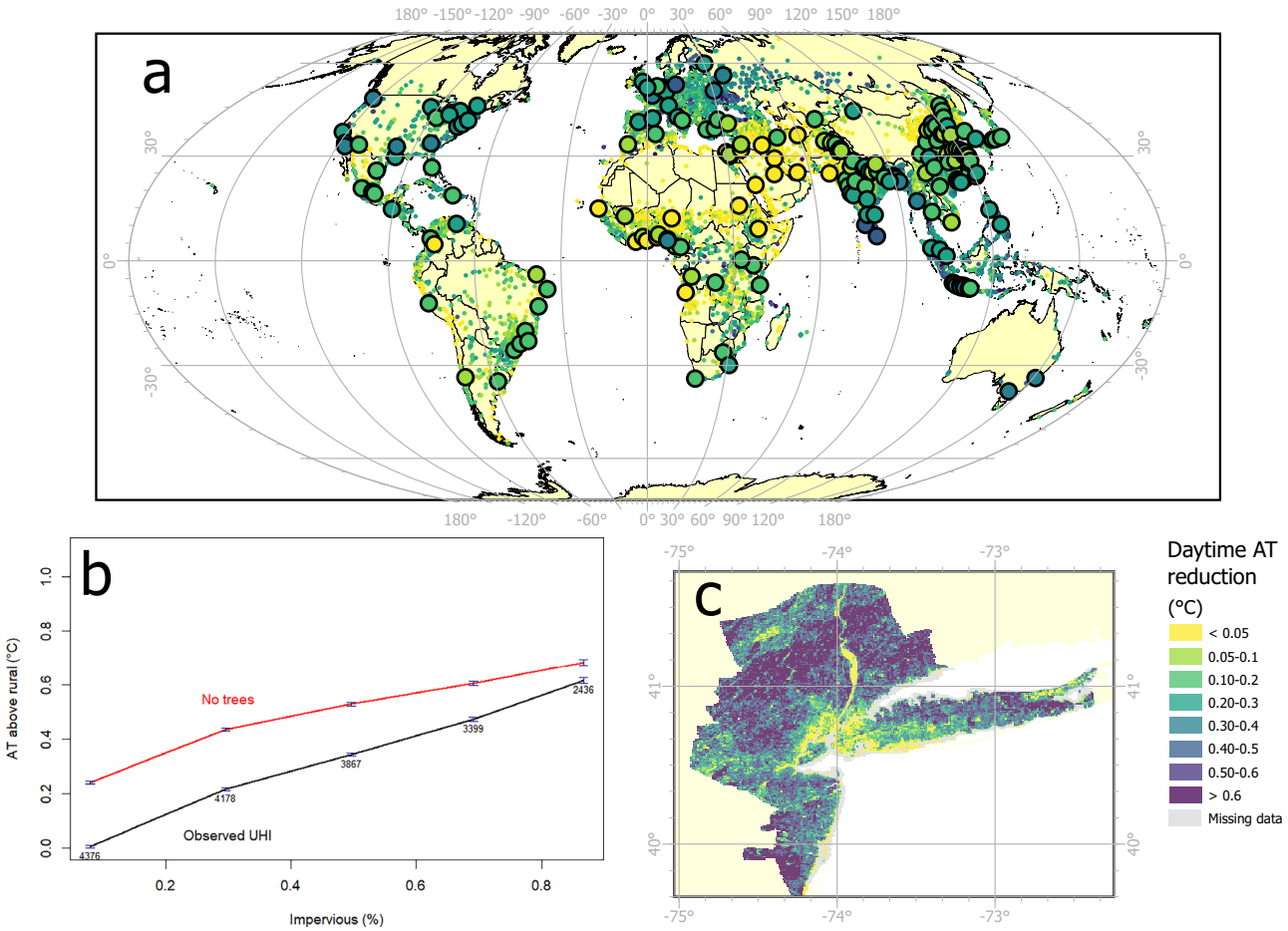

Fig. 4 | The reduction in daytime summer air temperatures (AT) by trees. a The average population-weighted reduction in air temperature (AT) for 8919 Functional Urban Areas (FUAs), compared to a counterfactual case of no tree canopy cover. FUAs with a population greater than 3 million are drawn with bigger circles; remaining FUAs are shown with small circles. **b** Within FUAs in humid climates, the average observed urban heat island (UHI) effect as a function of impervious surface nearby (black), as well as the estimate of AT without tree cover (red). The difference between the two lines is the reduction in AT by trees. Error bars are the standard error of the mean. Also shown are the number of FUAs in each impervious surface category. **c** The reduction in AT within the New York City FUA illustrates that the cooling effect of trees varies substantially. In forested biomes, dense urban areas have lower tree cover and hence less cooling by trees than suburban or rural areas.

The importance of scale and metric

To quantify spatial variation at scales smaller than 1 km that is not accounted for by our global statistical model, we calibrated a process-based model, i-Tree Cool Air, at a 30 m resolution for three case study cities of diverse levels of aridity: Phoenix, US (arid); Lisbon, Portugal (semi-arid); and Gothenburg, Sweden (humid). Results reveal substantial variation in total cooling at scales smaller than 1 km, as shown in an example from the Phoenix FUA (Supplementary Fig. 4). Using our global, 1 km resolution statistical model, total cooling varies from 0 °C to >0.6 °C for this FUA (Supplementary Fig. 4A), which includes the municipalities of Phoenix, Scottsdale, and Tempe. Total cooling within just one of our 1 km analysis cells (outlined in purple in Supplementary Fig. 4A), as estimated at a 30 m resolution by i-Tree Cool Air, varies widely. Total cooling varies from 0 °C to more than 0.6 °C among individual properties and roads (Supplementary Fig. 4B), driven by fine-scale patterns of tree cover. At the 1 km scale, the coefficient of variation (CV) was greater in more arid climates (Supplementary Fig. 4C). In all three FUAs, the i-Tree Cool Air model estimates substantial variation at the 30 m scale. This fine-scale variation is missing from our global model, which means that while we may be capturing average patterns of cooling by trees, we are likely underestimating the variation in the individual exposure to the heat-mitigation benefits of trees.

The magnitude of total cooling by trees is also highly dependent on the metric used. Here, for our global assessment, we focus our analysis on summer daytime AT. However, AT is not necessarily the most human health-relevant metric of heat stress, as it does not include (among other factors) the impact of humidity, solar radiation, and wind on human heat stress. To illustrate why AT as a metric may be underestimating the total reduction in heat stress provided by trees, we quantified with the i-Tree Cool Air model the Wet Bulb Globe Temperature (WBGT), an integrated metric that takes into account humidity, solar radiation, and wind speed and provides a more accurate measure of potential human heat stress[52].

The total cooling estimated in WBGT is greater than the cooling measured in summer AT (Table S1). WBGT cooling by trees is on average 3.1 times the AT total cooling, although the two are positively correlated ($r = 0.92$, $P < 0.001$). WBGT and AT are not linearly correlated, and the difference between them depended in our analysis on tree cover and the climate of the city. In general, the difference between WBGT and AT was the greatest in arid climates in pixels with high tree cover. In Phoenix, WBGT cooling is greater than AT cooling by 0.22 °C in the low tree cover 1 km cell, and by 2.09 °C in the high tree cover 1 km cell. In Gothenburg, at the other end of the aridity gradient, trees decrease WBGT by 0.19 °C more than AT in the low tree cover 1 km cell, and by 0.81 °C more than AT in the high tree cover 1 km cell.

https://doi.org/10.1038/s41467-026-71825-x

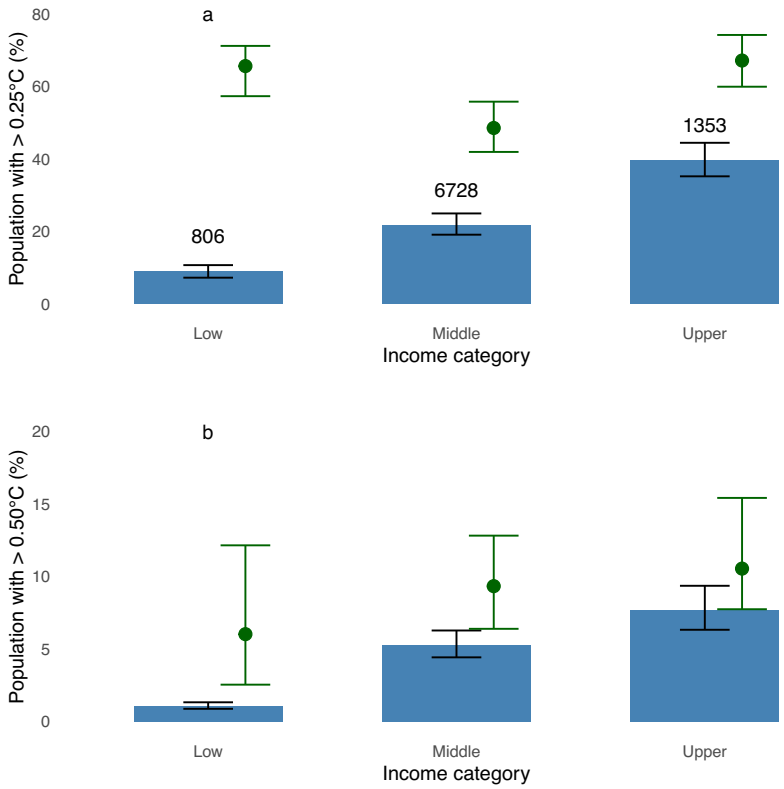

Fig. 5 | Urban population (%) receiving a reduction in air temperature from urban forests of more than 0.25 °C (a) or more than 0.5 °C (b), by income category. Income groups are defined by the country-level income category as defined by the World Bank using per-capita income (Low <USD 1145, Middle USD 1145–14,005, Upper >14,005 USD). The average current reduction by trees is shown with blue bars, while the average maximum plausible future reduction is shown with a green point. Error bars are the standard error of the population estimate. Also shown are the number of FUAs in each income category.

Discussion

Compared to the magnitude of the UHI, we find the world's urban forests deliver a substantial amount of cooling. Globally, urban tree canopy mitigates 48.6% (SUE algorithm) or 41.3% (buffering algorithm) of the maximum potential UHI. Urban areas will grow substantially over the 21st century, and some studies forecast that this will further increase the extent and magnitude of the UHI[53]. One uncertainty is how the urban tree canopy will change over time. Some studies suggest that at least in the Global North, urban expansion and an increase in UHI are associated with an increase in urban tree canopy[54], while other studies find broader increases in heat stress and decreases in greenness in cities[55]. Our scenario of maximum plausible urban tree cover shows that urban tree cover could almost double (from 18% to 33%), resulting in substantial additional heat-mitigation potential through urban greening.

However, tree canopy cover and its cooling benefits are unequally distributed. One principal reason is variation in aridity. Whether a climate is humid or arid controls which biome is naturally dominant (e.g., tree, grassland, desert)[56], and for trees, impacts their height and canopy width[57]. This leads to the amount of tree canopy cover varying between climates, and therefore, the amount of tree cooling benefits. Total tree cooling is greater in FUAs in humid climates than in arid climates, because some of the world's hottest cities in arid climates have relatively little tree cover. However, the TCE efficiency is greater in arid climates than in urban climates, meaning that, all else being equal, a 10% increase in tree cover in arid climates decreases AT more than in humid climates. This may be because humid climates have more water vapor in the atmosphere, and hence heat up and cool down more slowly than drier air[58]. Alternatively, it may be because trees in arid climates, especially those that are irrigated, can have high rates of transpiration, increasing localized cooling[59].

Tree cooling benefits are unequal in other respects as well. On average, total cooling by trees is greater in areas with low population, in suburbs and exurbs, and less in more densely populated city centers where the UHI is the greatest. This trend has been reported earlier in the US[25] and occurs because in neighborhoods with high impervious surface cover, there is less space for trees. Tree cooling is greater in upper-income countries than in low-income countries, which, on average, have less access to air conditioning and greater vulnerability during heat waves[60]. This supports the viewpoint of urban forests as an amenity that societies with more resources are better able to create[61]. Thus, the current inequitable distribution of trees limits their ability to provide cooling services to those most in need.

The magnitude of urban forest cooling appears modest compared with the magnitude of future increases in summer temperatures due to climate change, being 11% as large. We find that even under our maximum plausible tree-planting scenario, the cooling benefit from urban trees would only be 19% of the magnitude of future climate change. As such, current and plausible future urban tree canopies are unlikely to mitigate a substantial portion of the impacts of climate change. This suggests that a large-scale reduction in fossil fuel emissions to moderate the background global warming will be critical for protecting urban residents from future extreme heat. While further expansion of urban tree canopy can serve as an adaptation strategy in particular places, especially for vulnerable people, it will clearly not offset most of the warming caused by climate change. Urban tree canopy

enhancement should thus be seen as only one part of heat action planning by communities[62].

Our analysis quantifies some of the limits of urban tree canopies' ability to cool cities. One limit is physiological. TCE varies by climate and urban form, and other studies suggest it varies by species[63], but it is finite. Given surface energy budget constraints[5] there is a limit to how much tree cover can reduce near-surface air temperature by shading impervious surfaces (decreasing input of energy from solar radiation) or increasing transpiration (enhancing evaporative dissipation of heat). Another limit is practical. Planting trees in an urban environment can compete with other land uses, which is an expensive proposition in urban environments where land is valuable. However, proper urban planning and the use of space-sharing techniques (e.g., green roofs) can partially overcome this constraint and allow for neighborhoods that are both relatively dense and green[64].

Despite these limits on the total cooling ability of urban forests, our research suggests that urban tree cooling benefits could roughly double under our maximum plausible planting scenario, from a population-weighted average of 0.15 °C to 0.30 °C. Our results suggest future efforts to expand tree canopy have the greatest heat-mitigation benefits when targeted at more densely populated areas that currently have low levels of tree cover. These high-priority areas are located disproportionately in low-income countries. Moreover, arid and semi-arid areas have the greatest tree canopy efficiency and should be a focus of tree-planting efforts, to the extent water resources allow[58]. The greatest return on investment of tree planting for heat mitigation is in densely populated areas (>5000 people/km^2) in low-income countries, where the current canopy is lowest and plausible gains are the highest, and in arid regions where tree cooling efficiency is the greatest. Through targeted urban greening efforts, urban policy-makers can make the cooling benefits of the world's urban forests more equitable.

Methods

Our analysis workflow is shown in Fig. 1. Below, we describe our analysis in seven sections: (1) Data sources; (2) GIS processing; (3) the global 1 km empirical model; (4) global scenarios analyzed with the empirical model; (5) the high-resolution process model; (6) estimation of UHI; and (7) estimation of climate change impacts.

Data sources

We synthesized multiple input data sources, choosing input datasets that are as close in time as possible to 2019, the last year available year of a gridded estimate of air temperature (AT) by Zhang et al.[65] that is central to our analysis.

Our urban area definition is the functional urban area (FUA)[49]. This definition has the advantage of being applied in a consistent manner globally and includes both the central city and contiguous commuting zones. Urban area polygons were obtained from the Global Human Settlements Layer's 2019 boundary file (R2019A)[66], which was estimated using 2015 population data. Note that the GHS Urban Centre Database 2025[67], which includes an updated FUA boundary file, based upon 2023 population data, was released as this manuscript was being finalized, and so was not available for use in our analysis. As the urban population has grown between 2015 and 2023, the latter urban boundary is slightly wider, but broadly similar in shape and form, and it is unlikely that our results would have been substantially different using the GHS Urban Centre Database 2025. During statistical processing, to have statistically stable estimates of the mean air temperature in each FUA, we limited our study to large FUAs with at least 10 cells (roughly 10 km^2), giving us a total of 8919 FUAs with an estimated total population in 2020 of 3.6 billion. This is 86% of the total global urban population, as estimated by the UN Population Division[68].

Our population dataset for this project was taken from Landscan[69] for 2020. Landscan is one of the most spatially resolved of global population datasets, interpolating census estimates of population using other ancillary datasets such as information on infrastructure and nighttime lights. Comparison studies suggest it does better at resolving patterns of urban population than other globally available population grids, particularly in cities in lower-income countries[70]. The spatial resolution of the population grid became our common analysis grid, described in the next section.

For landcover, we used the Worldcover 10m v100 dataset[71], which provides consistent land cover information globally for the year 2020. Worldcover maps 11 land cover classes. For this analysis, we grouped as "tree cover" the "tree cover" and "mangrove" categories of Worldcover.

To estimate air temperature (AT), we used a recently developed urban-resolving gridded 1-km product based on a spatially varying coefficient model with sign preservation and combines ground-based AT measures with satellite observations by Zhang et al.[65] Summer average maximum and minimum AT were calculated for each 1 km grid within the FUAs based on average daily values for June, July, and August of 2015–2019 for the Northern hemisphere and December, January, and February for the Southern hemisphere. We limit our analysis to 2019 to avoid AT anomalies related to the COVID-19 lockdowns for 2020.

We estimated summertime land surface temperature (LST) for comparison with the AT. To do so, we used the MODIS Aqua daily LST scenes, which are available for roughly 01:30 and 13:30 local time. The Northern Hemisphere and Southern Hemisphere summer months were analyzed, like the AT analysis, and pixel-level quality control flags were used to only consider pixels with <3K error before averaging. Code used to analyze the MODIS data, including details of scenes accessed, is available in our code repository.

In addition to the raw LST and AT, we calculated the temperature anomaly, defined as the value in a pixel minus the mean temperature, calculated within a FUA. This centers the statistical distribution of temperature on zero and allows comparison of land-use effects on temperature anomaly among FUAs with different mean temperatures.

The Aridity Index (AI) is defined by the UN Environment Program (UNEP) as the ratio of precipitation to potential evapotranspiration[72], and measures how dry or humid a climate is. Values below 0.20 are considered arid, values between 0.2 and 0.5 are considered semi-arid, values between 0.5 and 0.65 are dry subhumid, and values above 0.65 are considered humid climates. Specifically, we used the recent 30 arcsec resolution (v3) maps of AI[73]. Where categorical variables were needed for statistical analysis, we sometimes used the traditional UNEP groupings (arid, semi-arid, dry subhumid, and humid) and sometimes, for reasons of statistical power, grouped them into two categories: dry (arid and semi-arid) and humid (dry subhumid and humid subcategories).

Another common way to measure climate is through Koppen Climate Zones[74]. Here, we used the most recent, 1 km resolution maps of current Koppen Climate Zones[75]. To have a stable estimate of mean temperature within Koppen climate zones, we grouped categories with <500 grid cells (i.e., 500 km^2 of total area) globally within them to the next nearest category. For instance, there were a few FUAs in the DfD category (extreme cold subarctic climate), so these FUAs were grouped with the DfC category (subarctic climate). Similarly, for some statistical analyses, we used the next level in the hierarchy (e.g., the Df category, continental climates with no dry season).

As a measure of the level of economic development within a country and its ability to invest in urban tree planting and maintenance, we used per-capita income from the World Bank, in USD2020 Purchasing Power Parity[76]. We then used the World Bank's classification thresholds to divide countries into Low Income, Middle Income (incorporating the Lower Middle Income and Upper Middle-Income categories of the World Bank), and Upper Income. We chose to use

country-level economic data rather than finer-scale global datasets using subnational jurisdictions (e.g., at Admin Level 2) because there were spatial difficulties consistently and correctly aligning FUA boundaries with the subnational jurisdiction boundaries, since FUAs often contain multiple subnational jurisdictions, and these jurisdictions often are only partially within a FUA.

As a potential explanatory variable helping predict AT, we included the best global estimate of Anthropogenic heat currently available[77], which predicts anthropogenic heat in 2010 at 1 km resolution.

We used downscaled projections from the Coupled Model Intercomparison Project, Phase 6 (CMIP6) climate and earth system models[78]. See the section on Climate Analysis below for details on processing.

As part of our high-resolution analysis using the i-Tree Cool Air model, we needed high-resolution meteorological information. We used the US National Oceanic and Atmospheric Administration (NOAA)'s National Centers for Environmental Information (NCEI) meteorological data (integrated surface database, hourly time step) and the US National Aeronautics and Space Administration (NASA) Giovanni IMERG precipitation data (area averaged, hourly time step)[79] to simulate conditions across three focal FUAs (Gothenburg, Sweden; Lisbon, Portugal; and Phoenix, US; see details below for FUA selection). Digital elevation model inputs were obtained from the 30 m resolution Copernicus GLO-30 Digital Elevation Model[80]. Maps of tree cover and impervious cover were obtained by resampling Worldcover 10 m into 30 m pixels of fractional coverage, and this became the scale of our i-Tree Cool Air analysis.

GIS processing

We collated input data for FUAs, land cover, Koppen climate zone, AT, and LST in Google Earth Engine to a common grid stored in JSON format, matching the cell size (30 arcsec, around 1 km at the equator) and extent of the population data. We chose to keep the common grid in this latitude and longitude (geographic) projection, to match the population and other layers most precisely (e.g., land cover) that come in this projection, rather than reproject all the datasets to an equal area projection and introduce error. When needed for areal calculations at a few specific points in the processing, we used a Mollweide Equal Area projection.

Supporting global datasets (i.e., Aridity Index, per-capita income, anthropogenic heat, and climate projection information) were collated in ArcGIS Pro 3.5.0 and exported to a CSV dataset for merging with the main database in the language *R* (v4.5.0) and further statistical analysis. Across the 8919 FUAs analyzed in this study, there were 4.7 million cells in the common analysis grid.

For the higher spatial resolution i-Tree Cool Air model, we stratified our analysis over three FUAs in three contrasting climates: Phoenix (Arid); Lisbon (Semi-Arid); and Gothenburg (Humid). Within each FUA, we chose three ~1 km grid cells from the common analysis grid, which had low (bottom quartile), moderate (near median), and high (top quartile) levels of tree cover. Within each of these nine cells (3 FUAs × 3 cells/FUA), we collated the secondary datasets needed for this model (see the "Data sources" section) and processed them at a 30 m resolution. A National Land Cover Database (NLCD) Class was derived for each pixel based on the 30 m resolution Worldcover map, with urban class 21 assigned when impervious cover (IC) was less than or equal to 20%, urban class 22 assigned for IC between 20% and 50%, urban class 23 assigned for IC between 50% and 80%, and urban class 24 assigned for IC ≥80%.

Global 1 km empirical model

Statistical analysis was conducted in *R* version 4.5.0, using *RStudio* version 2025.05.1 Build 513. Where partially missing data occurred (i.e., 1 km cells with a valid estimate for some but not all variables), these cells were excluded from a particular statistical analysis if one of the variables involved in that analysis was missing.

As part of our descriptive analysis of the dataset, we estimated population density (people/km^2) and then constructed population bins, within which we calculated average population-weighted tree canopy cover and impervious surface cover as a function of population density by country-level income category (upper income, middle income, or low-income) and aridity. Population bins were constructed based on global quintiles of population density, but with the boundaries adjusted to align with round numbers. Note that when constructing summary statistics for subgroups (e.g., for specific levels of country income and climate), not all population bins were present for all FUAs, and so were left blank in Fig. 3.

Our model relating land cover, most especially tree cover, to temperature at the 1 km scale was fit empirically using a hierarchical regression approach. First, at the FUA level, the LST and AT anomalies were estimated by accounting for the FUA-level mean effect. This centers the distribution of LST and AT on zero, increases the normality of the distribution, and aligns FUAs with different mean temperatures so that the within-FUA effect of land cover on temperature can be comparably analyzed. Second, AT and LST anomalies at the 1 km^2 were treated as response variables of within-FUA variation, to be predicted by a set of potentially explanatory variables: fractional land cover, anthropogenic heat, aridity index, and Köppen Climate zone. Note that while the original Worldcover land cover was categorical at a 10 m resolution, when summed up to the 1 km^2 of our common grid, the sum can be expressed as the fraction of the 1 km^2 that was a certain land cover class. After examination of Pearson correlation coefficients among land cover categories, we grouped land cover categories into six categories to avoid any potential issues of multicollinearity: water, tree cover, cropland, sparse vegetation, bare, and impervious.

Exploratory analysis indicated that the categorical aridity index (AI) classes explained more of the variation in AT and LST anomalies, so these AI classes were used in our final model. Explanatory terms related to land cover and anthropogenic heat were then only added to the model if there was a substantial increase in explanatory power of the model, defined as an increase in adjusted R^2 of more than 1%. We allowed the slope of model parameters to vary within each AI class. Interaction terms were allowed to enter if the main effects were already in the final model.

After an initial model was fit, we calculated the model residuals and examined patterns in the spatial autocorrelation in model errors, which poses a problem for assumptions of independence in linear regression[81]. Spatial autocorrelation in model residuals was greater when cells were within 3 km of each other. We therefore chose to randomly draw a subset of our global datasets, with the constraint that sampled cells were at least 3 km from one another, using the *spatstat.geom* library for *R*'s function *nndist*. This subset was used to fit the final regression presented in this paper.

Global scenarios

The empirical regression model, which was developed for observed data (baseline case), was used to estimate daytime LST and AT for three scenarios.

First, we defined a scenario where tree cover increases 10%, assuming a 10% increase in tree cover in each 1 km pixel. The purpose of this scenario is to calculate tree cooling efficiency (TCE), the effect on temperature of a 10% increase in tree cover. The scenario is not meant to imply that a 10% increase in tree cover is feasible or likely within a particular cell, but is rather a hypothetical calculation designed to allow the estimation of TCE.

Second, we defined a scenario where the tree canopy is totally lost, assuming a complete loss of tree cover in each 1 km cell. The purpose of this scenario is to estimate the total tree cooling, the

aggregate reduction in temperature due to all the tree cover in a 1 km pixel. Such a total loss of tree canopy cover is not likely, but this scenario allows estimation of the LST and AT in the counterfactual case of no tree cover.

Third, we estimated the impact of the maximum plausible increase in tree cover on LST and AT. The goal was to estimate how much additional cooling benefit urban tree canopy could have. To make our results more realistic, we constrained tree canopy increases in two ways: (1) a physical constraint (trees can generally only be planted in non-impervious surfaces) and (2) a social/political/climatic constraint (planting trees is constrained by numerous other considerations, including competing land uses, landowner preferences, zoning and building codes, and climatic conditions)[22]. The physical constraint was incorporated by ensuring that the maximum plausible increase in tree cover did not exceed the pervious surface area within the 1 km pixel. The social/political/climatic constraint was incorporated by dividing the landscape into five impervious surface categories (0–20%, 20–40%, 40–60%, 60–80%, 80–100%) to reflect the different landscape contexts from lightly settled suburbs to dense urban core. Moreover, each pixel was assigned to an AI category. The social/political/climatic constraint was then defined at the 90th percentile of observed tree cover in each impervious surface category for the AI category. That is, the maximum plausible increase target was set at the 90th percentile of tree cover for pixels with similar aridity and with similar landscape contexts (imperviousness), or the maximum tree cover allowed given the pervious surface within the 1 km pixel, whichever is less.

In all three scenarios, predicted LST and AT were analyzed by comparing them to the baseline case. Note that in all three scenarios, the other land cover in a 1 km cell needs to change so that the total land cover sum is 100%. For all three scenarios, other land covers were expected to increase or decrease (except for water and cropland, which were assumed to be constant) in proportion to their occurrence in the cell. In rare cases when a cell was already almost entirely tree cover, we used the proportions of other land covers found at the FUA scale. Specifically, we gave weight to FUA-level information on the proportions of other land covers using Eq. (1):

$$Tree.cover_{pixel}\ FUA.info + (1 - Tree.cover_{pixel})\ Pixel.info \quad (1)$$

When the pixel-level tree cover is close to zero, our model primarily uses information on the frequency of other land covers at the pixel level. Conversely, when the pixel-level tree cover is close to one (i.e., there are no other land cover types within that pixel), our model uses primarily information on the frequency of other land covers at the FUA level.

High-resolution process model

We used the i-Tree Cool Air model to simulate hourly 2-m high AT and humidity between 2015 and 2019 using a soil–vegetation–atmosphere transfer scheme for its water and energy balances[82]. The model is distributed within the i-Tree HydroPlus suite, and revision 1659 was used for this study. The model has been spatially validated for summer AT and humidity in Syracuse, New York, USA[82] and Napoli, Italy, both at multiple meteorological stations during extreme heat conditions[83] and against eddy covariance tower data for sensible and latent heat fluxes during both wet (2015) and dry (2017) summer periods[84]. For each timestep, the model assimilated observed meteorological data from a station-containing pixel and solved for the upper boundary layer AT and humidity across the domain. Meteorological inputs were drawn from the station closest to each of the nine 1 km cells analyzed by the i-Tree Cool Air model (see GIS processing section for the selection of these 9 sites). It then uses these boundary conditions with land cover-dependent energy and water properties and aerodynamic coupling to determine 2-m AT and humidity across the full modeling domain. It also estimates wet bulb globe temperature (WBGT). To determine water availability in each pixel, the model uses terrain elevation to laterally redistribute subsurface water and represent soil wetness based on the topographic index and TOPMODEL theory[85]. The model operates in coordination with the i-Tree Hydro model[86] included in HydroPlus, which provides a statistically distributed representation of topographic index bins to simulate temporally varying soil moisture deficit across the domain using hydrologic similarity. Following Pace et al.[83], we calibrated the model using data from two full water years (October 1, 2017–September 30, 2019) to estimate three groundwater parameters: initial groundwater drainage rate, transmissivity at saturation, and hydraulic conductivity decay scaling parameter, based on an average soil moisture deficit for each FUA. These calibrated values were then passed to the i-Tree Cool Air model for spatially explicit simulation of water and energy fluxes at the pixel level.

Analysis with i-Tree Cool Air was focused on contrasting the current AT with what would be observed in a counterfactual case of no tree cover (i.e., the total tree canopy loss scenario). The tree cover was replaced with the proportional mix of other land covers found in the 1-km cell being analyzed. We compared the AT results from the i-Tree Cool Air model with the empirical global model, looking at how the coefficient of variation (CV) of the two models' outputs differed. The goal was to quantify the spatial variation in AT at fine spatial scales that was necessarily missing from the 1 km empirical model. We also examined the relationship between WBGT (only estimated with the i-Tree Cool Air model) and AT estimates from the empirical global model, with the goal of quantifying whether, under the complete canopy loss scenario, the magnitude of change in WBGT was greater or less than the magnitude of change in AT.

UHI estimation

We estimated the UHI intensity for LST and AT by subtracting the LST and AT values from a rural reference value for each FUA. There are several algorithms that are used to define a relevant rural reference value. Here, we used two algorithms to define the rural reference value and compared the estimated UHI using both. Both algorithms were applied globally to allow direct comparison with regression-based tree-cooling estimates.

One algorithm is called the simplified urban extent. Here, we calculated the average LST or AT for each FUA based on all non-urban, non-water, and non-snow, ice pixels, as defined by the ESA Worldcover data. This is an application of the simplified urban extent (SUE) algorithm[87], used to estimate the UHI without creating explicit buffers.

Another algorithm is based on a typical buffering approach. We generated normalized buffers around each FUA following Chakraborty et al. (2021)[88], and then calculated the average LST or AT of the non-urban, non-water, and non-snow, ice pixels, as defined by the ESA Worldcover data in these buffers. Additionally, pixels in the buffer that are higher or lower than 50 m above the median elevation of the urban area it surrounds are removed because elevation is a strong controller of AT.

Using each algorithm, we estimated the UHI intensity for all large FUAs globally. Using predictions from the global 1 km empirical model for the "Total tree canopy loss" scenario, we had estimates of how much hotter each FUA would be without any tree cover. We then calculated, for each FUA, the maximum potential UHI as the sum of the currently observed UHI intensity and the current cooling benefits provided by tree cover (i.e., −1 times the ΔAT under the total tree canopy loss scenario). The maximum potential UHI represents an estimate of what the UHI would be if there were hypothetically no tree canopy cover.

Climate change impacts

We compared the impact of trees and UHI effects to the projected impacts of mid-century global warming on summer afternoon

temperature changes using a constrained ensemble of Coupled Model Intercomparison Project, Phase 6 (CMIP6) climate and earth system models[78]. Specifically, we used the downscaled NASA NEX GDDP[89] monthly average daily maximum ('tasmax') temperature data from June–July–August for the Northern hemisphere and December–January–February for the Southern hemisphere. For each downscaled climate model, we calculated the average afternoon summer temperature change at mid-century (2041–2060) in the SSP2–4.5 scenario relative to the World Meteorological Organization climate baseline period (1981–2020). We chose the SSP2–4.5 scenario as it is a moderate growth, 'middle of the road' emissions pathway[50] estimated to most closely follow current and pledged global greenhouse gas emissions policies[90]. Some CMIP6 models may show unrealistically high climate sensitivity, so we constrain the ensemble to the 15 downscaled NEX GDDP CMIP6 models with 'likely' Equilibrium Climate Sensitivity (Table S1)[91]. Global raster data on the average afternoon summer temperature change was then collated to the FUA level by calculating in ArcGIS Pro the average change within each FUA polygon.

Reporting summary

Further information on research design is available in the Nature Portfolio Reporting Summary linked to this article.

Data availability

All datasets generated in this study have been deposited in Data Dryad under the https://doi.org/10.5061/dryad.905qfttz0.

Code availability

All code used in this analysis is available on Data Dryad under the https://doi.org/10.5061/dryad.905qfttz0.

References

1. Burkart, K. G. et al. Estimating the cause-specific relative risks of non-optimal temperature on daily mortality: a two-part modelling approach applied to the Global Burden of Disease Study. *Lancet* **398**, 685–697 (2021).
2. Rizwan, A. M. & Dennis, L. Y. A review on the generation, determination and mitigation of Urban Heat Island. *J. Environ. Sci.* **20**, 120–128 (2008).
3. Deilami, K., Kamruzzaman, M. & Liu, Y. Urban heat island effect: a systematic review of spatio-temporal factors, data, methods, and mitigation measures. *Int. J. Appl. Earth Obs. Geoinf.* **67**, 30–42 (2018).
4. McDonald, R. I., Kroeger, T., Zhang, P. & Hamel, P. The value of US urban tree cover for reducing heat-related health impacts and electricity consumption. *Ecosystems* **23**, 137–150 (2019).
5. Oke, T. R. The energetic basis of the urban heat island. *Q. J. R. Meteorol. Soc.* **108**, 1–24 (1982).
6. Unger, J. Intra-urban relationship between surface geometry and urban heat island: review and new approach. *Clim. Res.* **27**, 253–264 (2004).
7. Tzavali, A., Paravantis, J. P., Mihalakakou, G., Fotiadi, A. & Stigka, E. Urban heat island intensity: a literature review. *Fresenius Environ. Bull.* **24**, 4537–4554 (2015).
8. Yang, Q. et al. A global urban heat island intensity dataset: generation, comparison, and analysis. *Remote Sens. Environ.* **312**, 114343 (2024).
9. McDonald, R. I., Kroeger, T., Boucher, T., Wang, L. & Salem, R. *Planting Healthy Air: A Global Analysis of the Role of Urban Trees in Addressing Particulate Matter Pollution and Extreme Heat* (The Nature Conservancy, 2016).
10. EPA. *Reducing Urban Heat Islands: Compendium of Strategies (Draft)* (Environmental Protection Agency, 2014).
11. Huang, C. et al. Projecting future heat-related mortality under climate change scenarios: a systematic review. *Environ. Health Perspect.* **119**, 1681–1690 (2011).
12. Lee, H. et al. IPCC, 2023: Climate Change 2023: Synthesis Report, Summary for Policymakers. In *Contribution of Working Groups I, II and III to the Sixth Assessment Report of the Intergovernmental Panel on Climate Change* (eds. Core Writing Team, Lee, H. & Romero, J.) (IPCC, 2023).
13. IPCC. *Climate Change 2022—Impacts, Adaptation and Vulnerability: Working Group II Contribution to the Sixth Assessment Report of the Intergovernmental Panel on Climate Change*. (Cambridge University Press, 2023).
14. Yin, C. et al. Changes in global heat waves and its socioeconomic exposure in a warmer future. *Clim. Risk Manag.* **38**, 100459 (2022).
15. Esper, J., Torbenson, M. & Büntgen, U. 2023 summer warmth unparalleled over the past 2,000 years. *Nature* **631**, 94–97 (2024).
16. Gasparrini, A. et al. Projections of temperature-related excess mortality under climate change scenarios. *Lancet Planet. Health* **1**, e360–e367 (2017).
17. Matthies, F., Bickler, G., Marin, N. & Hales, S. *Heat–Health Action Plans* (WHO Regional Office for Europe, Copenhagen, 2008).
18. Boeckmann, M. & Rohn, I. Is planned adaptation to heat reducing heat-related mortality and illness? A systematic review. *BMC Public Health* **14**, 1112 (2014).
19. Kroeger, T., McDonald, R. I., Boucher, T., Zhang, P. & Wang, L. Where the people are: current trends and future potential targeted investments in urban trees for PM10 and temperature mitigation in 27 U.S. cities. *Landsc. Urban Plan.* **177**, 227–240 (2018).
20. Paschalis, A., Chakraborty, T., Fatichi, S., Meili, N. & Manoli, G. Urban forests as main regulator of the evaporative cooling effect in cities. *AGU Adv.* **2**, e2020AV000303 (2021).
21. Ziter, C. D., Pedersen, E. J., Kucharik, C. J. & Turner, M. G. Scale-dependent interactions between tree canopy cover and impervious surfaces reduce daytime urban heat during summer. *Proc. Natl. Acad. Sci. USA* **116**, 7575–7580 (2019).
22. McDonald, R. et al. Current inequality and future potential of US urban tree canopy cover for reducing heat-related mortality, morbidity and electricity consumption. *npj Urban Sustain.* **4**, Article 18 (2024).
23. Zhang, H. et al. Unequal urban heat burdens impede climate justice and equity goals. *Innovation* **4**, 100488 (2023).
24. Nowak, D. J. & Greenfield, E. J. The increase of impervious cover and decrease of tree cover within urban areas globally (2012–2017). *Urban For. Urban Green.* **49**, 126638 (2020).
25. McDonald, R. I. et al. The tree cover and temperature disparity in US urbanized areas: quantifying the association with income across 5,723 communities. *PLoS ONE* **16**, e0249715 (2021).
26. Hsu, A., Sheriff, G., Chakraborty, T. & Manya, D. Disproportionate exposure to urban heat island intensity across major US cities. *Nat. Commun.* **12**, 2721 (2021).
27. Benz, S. A. & Burney, J. A. Widespread race and class disparities in surface urban heat extremes across the United States. *Earth's Future* **9**, e2021EF002016 (2021).
28. Rigolon, A., Browning, M. H., Lee, K. & Shin, S. Access to urban green space in cities of the Global South: a systematic literature review. *Urban Sci.* **2**, 67 (2018).
29. Venter, Z. S., Shackleton, C. M., Van Staden, F., Selomane, O. & Masterson, V. A. Green Apartheid: urban green infrastructure remains unequally distributed across income and race geographies in South Africa. *Landsc. Urban Plan.* **203**, 103889 (2020).
30. Pedlowski, M. A., Da Silva, V. A. C., Adell, J. J. C. & Heynen, N. C. Urban forest and environmental inequality in Campos dos Goytacazes, Rio de Janeiro, Brazil. *Urban Ecosyst.* **6**, 9–20 (2002).
31. Nghiem, L. T. et al. Equity in green and blue spaces availability in Singapore. *Landsc. Urban Plan.* **210**, 104083 (2021).

32. Chakraborty, T. Higher urban heat hazard in wealthier neighborhoods in the Global South. Preprint at https://doi.org/10.21203/rs.3.rs-4461139/v1 (2024).
33. Zhou, D. et al. Satellite remote sensing of surface urban heat islands: progress, challenges, and perspectives. *Remote Sens.* **11**, 48 (2018).
34. Schwaab, J. et al. The role of urban trees in reducing land surface temperatures in European cities. *Nat. Commun.* **12**, 6763 (2021).
35. Venter, Z. S., Chakraborty, T. & Lee, X. Crowdsourced air temperatures contrast satellite measures of the urban heat island and its mechanisms. *Sci. Adv.* **7**, eabb9569 (2021).
36. Du, M. et al. Daytime cooling efficiencies of urban trees derived from land surface temperature are much higher than those for air temperature. *Environ. Res. Lett.* **19**, 044037 (2024).
37. Hu, Y. et al. Comparison of surface and canopy urban heat islands within megacities of eastern China. *ISPRS J. Photogramm. Remote Sens.* **156**, 160–168 (2019).
38. Yang, Q. et al. Global assessment of urban trees' cooling efficiency based on satellite observations. *Environ. Res. Lett.* **17**, 034029 (2022).
39. Leng, S., Sun, R., Yan, M., He, H. & Chen, L. Interannual variability and spatial diversification of global urban tree cooling effects. *Environ. Int.* **192**, 109044 (2024).
40. Zhao, J., Zhao, X., Wu, D., Meili, N. & Fatichi, S. Satellite-based evidence highlights a considerable increase of urban tree cooling benefits from 2000 to 2015. *Glob. Change Biol.* **29**, 3085–3097 (2023).
41. Chakraborty, T., Venter, Z. S., Qian, Y. & Lee, X. Lower urban humidity moderates outdoor heat stress. *AGU Adv.* **3**, e2022AV000729 (2022).
42. Ibsen, P. C. et al. Urban tree cover provides consistent mitigation of extreme heat in arid but not humid cities. *Sustain. Cities Soc.* **113**, 105677 (2024).
43. Hwang, B., Sou, H.-D., Oh, J.-H. & Park, C.-R. Cooling effect of urban forests on the urban heat island in Seoul, South Korea. *PLoS ONE* **18**, e0288774 (2023).
44. Feyisa, G. L., Dons, K. & Meilby, H. Efficiency of parks in mitigating urban heat island effect: an example from Addis Ababa. *Landsc. Urban Plan.* **123**, 87–95 (2014).
45. Yin, Y. et al. Cooling benefits of urban tree canopy: a systematic review. *Sustainability* **16**, 4955 (2024).
46. Li, H. et al. Cooling efficacy of trees across cities is determined by background climate, urban morphology, and tree trait. *Commun. Earth Environ.* **5**, 754 (2024).
47. Su, Y. et al. Phenology acts as a primary control of urban vegetation cooling and warming: a synthetic analysis of global site observations. *Agric. For. Meteorol.* **280**, 107765 (2020).
48. McDonald, R. I. et al. Research gaps in knowledge of the impact of urban growth on biodiversity. *Nat. Sustain.* **3**, 16–24 (2020).
49. Dijkstra, L., Poelman, H. & Veneri, P. *The EU-OECD Definition of a Functional Urban Area (OECD Regional Development Working Papers, Issue 2019/11)* (OECD Publishing, 2019).
50. Riahi, K. et al. The Shared Socioeconomic Pathways and their energy, land use, and greenhouse gas emissions implications: an overview. *Glob. Environ. Change* **42**, 153–168 (2017).
51. Hausfather, Z., Drake, H. F., Abbott, T. & Schmidt, G. A. Evaluating the performance of past climate model projections. *Geophys. Res. Lett.* **47**, e2019GL085378 (2020).
52. Budd, G. M. Wet-bulb globe temperature (WBGT)—its history and its limitations. *J. Sci. Med. Sport* **11**, 20–32 (2008).
53. Huang, K., Li, X., Liu, X. & Seto, K. C. Projecting global urban land expansion and heat island intensification through 2050. *Environ. Res. Lett.* **14**, 114037 (2019).
54. Chen, J. et al. Contrasting effects of urbanization on vegetation between the Global South and Global North. *Nat. Sustain.* **8**, 373–384 (2025).
55. Ye, T. et al. Billions of people exposed to increasing heat but decreasing greenness from 2000 to 2022. *Innovation* **6**, 100870 (2025).
56. Woodward, F. I., Lomas, M. R. & Kelly, C. K. Global climate and the distribution of plant biomes. *Philos. Trans. R. Soc. Lond. Ser. B: Biol. Sci.* **359**, 1465–1476 (2004).
57. Lines, E. R., Zavala, M. A., Purves, D. W. & Coomes, D. A. Predictable changes in aboveground allometry of trees along gradients of temperature, aridity and competition. *Glob. Ecol. Biogeogr.* **21**, 1017–1028 (2012).
58. McDonald, R. I. et al. *Roots of Resilience: Using Trees to Mitigate Rising Heat in Arid, Frontline Communities* (The Nature Conservancy, 2024).
59. Winbourne, J. B. et al. Tree transpiration and urban temperatures: current understanding, implications, and future research directions. *BioScience* **70**, 576–588 (2020).
60. Davis, L., Gertler, P., Jarvis, S. & Wolfram, C. Air conditioning and global inequality. *Glob. Environ. Change* **69**, 102299 (2021).
61. Schwarz, K. et al. Trees grow on money: urban tree canopy cover and environmental justice. *PLoS ONE* **10**, e0122051 (2015).
62. Matthies, F. *Heat-health Action Plans: Guidance* (World Health Organization, 2008).
63. Rahman, M. A., Armson, D. & Ennos, A. A comparison of the growth and cooling effectiveness of five commonly planted urban tree species. *Urban Ecosyst.* **18**, 371–389 (2015).
64. McDonald, R. I. et al. Denser and greener cities: green interventions to achieve both urban density and nature. *People Nat.* **5**, 84–102 (2023).
65. Zhang, T., Zhou, Y., Wang, L., Zhao, K. & Zhu, Z. Estimating 1 km gridded daily air temperature using a spatially varying coefficient model with sign preservation. *Remote Sens. Environ.* **277**, 113072 (2022).
66. Marí Rivero, I. et al. *Urban Centre Database R2019A* (European Commission, Joint Research Centre (JRC), 2024).
67. Mari Rivero, I. et al. *GHS-UCDB R2024A—GHS Urban Centre Database* 2025 (European Commission, Joint Research Centre (JRC), 2025).
68. UNPD. *World Urbanization Prospects: The 2018 Revision* (United Nations Population Division, 2018).
69. Dobson, J. E., Bright, E. A., Coleman, P. R., Durfee, R. C. & Worley, B. A. LandScan: a global population database for estimating populations at risk. *Photogramm. Eng. Remote Sens.* **66**, 849–857 (2000).
70. Yin, X. et al. Which gridded population data product is better? Evidences from mainland Southeast Asia (MSEA). *ISPRS Int. J. Geo-Inf.* **10**, 681 (2021).
71. Zanaga, D. et al. ESA WorldCover 10 m 2020 v100 (European Space Agency, 2021).
72. Trabucco, A. & Zomer, R. *Global Aridity Index (Global-Aridity) and Global Potential Evapo-Transpiration (Global-PET) Geospatial Database* (CGIAR Consortium for Spatial Information, 2009).
73. Zomer, R. J., Xu, J. & Trabucco, A. Version 3 of the global aridity index and potential evapotranspiration database. *Sci. Data* **9**, 409 (2022).
74. Peel, M. C., Finlayson, B. L. & McMahon, T. A. Updated world map of the Köppen–Geiger climate classification. *Hydrol. Earth Syst. Sci.* **11**, 1633–1644 (2007).
75. Beck, H. E. et al. High-resolution (1 km) Köppen-Geiger maps for 1901–2099 based on constrained CMIP6 projections. *Sci. Data* **10**, 724 (2023).

76. Fantom, N. J. & Serajuddin, U. *The World Bank's Classification of Countries by Income*. World Bank Policy Research Working Paper (World Bank, 2016).
77. Varquez, A. C. G., Kiyomoto, S., Khanh, D. N. & Kanda, M. Global 1-km present and future hourly anthropogenic heat flux. *Sci. Data* **8**, 64 (2021).
78. Eyring, V. et al. Overview of the Coupled Model Intercomparison Project Phase 6 (CMIP6) experimental design and organization. *Geosci. Model Dev.* **9**, 1937–1958 (2016).
79. Liu, Z., Acker, J., Seiler, E. & Bryant, K. NASA Giovanni: Analyze, Compare, and Visualize 2000+ Earth Satellite and Model Variables Without Downloading Data and Software. (American Geophysical Union, 2024). https://agu.confex.com/agu/agu24/meetingapp.cgi/Paper/1619774.
80. European Space Agency. *Copernicus Global Digital Elevation Model* (*Distributed by Open Topography*) https://doi.org/10.5069/G9028PQB (2024).
81. McDonald, R. I. & Urban, D. L. Spatially varying rules of land-cover change: lessons from a case study. *J. Landsc. Urban Plan.* **74**, 7–20 (2006).
82. Yang, Y., Endreny, T. A. & Nowak, D. J. A physically based analytical spatial air temperature and humidity model. *J. Geophys. Res. Atmos.* **118**, 10,449–410,463 (2013).
83. Pace, R. et al. Mitigation potential of urban greening during heat-waves and stormwater events: a modeling study for Karlsruhe, Germany. *Sci. Rep.* **15**, 5308 (2025).
84. Guidolotti, G. et al. Impact of drought on cooling capacity and carbon sequestration in urban green area. *Urban Clim.* **59**, 102244 (2025).
85. Wang, J., Endreny, T. A. & Hassett, J. M. A flexible modeling package for topographically based watershed hydrology. *J. Hydrol.* **314**, 78–91 (2005).
86. Wang, J., Endreny, T. A. & Nowak, D. J. Mechanistic simulation of tree effects in an urban water balance model 1. *J. Am. Water Resour. Assoc.* **44**, 75–85 (2008).
87. Chakraborty, T. & Lee, X. A simplified urban-extent algorithm to characterize surface urban heat islands on a global scale and examine vegetation control on their spatiotemporal variability. *Int. J. Appl. Earth Observ. Geoinf.* **74**, 269–280 (2019).
88. Chakraborty, T., Sarangi, C. & Lee, X. Reduction in human activity can enhance the urban heat island: insights from the COVID-19 lockdown. *Environ. Res. Lett.* **16**, 054060 (2021).
89. Thrasher, B. et al. NASA global daily downscaled projections, CMIP6. *Sci. Data* **9**, 262 (2022).
90. Hausfather, Z. & Peters, G. P. Emissions—the 'business as usual's-tory is misleading. *Nature* **577**, 618–620 (2020).
91. Hausfather, Z., Marvel, K., Schmidt, G. A., Nielsen-Gammon, J. W. & Zelinka, M. Climate simulations: recognize the 'hot model'problem. *Nature* **605**, 26–29 (2022).

Acknowledgements

R.I.M., L.A.P., and M.M. were supported in this research by general funds from The Nature Conservancy's members and donors, as well as a grant from the Lyda Hill Philanthropies. T.C. was supported by the Earth and Environmental Systems Modeling program area of the U.S. Department of Energy (DOE) Office of Science's Biological and Environmental Research program through a DOE Early Career Award. Pacific Northwest National Laboratory is operated for the DOE by the Battelle Memorial Institute under contract DE-AC05-76RL01830. i-Tree Cool Air Model development was partly supported by the U.S. Forest Service National Urban and Community Forestry Advisory Council (USFS NUCFAC), grant 21-DG-11094200-242. M.E.R. received funding from Western Sydney University's Research Theme Program. We thank Deborah Balk and Arthur Gessler for early discussions about the framing of this research.

Author contributions

R.I.M. and T.C. designed the research jointly and led the statistical and remote sensing analysis, respectively. T.A.E. conducted the i-Tree Cool Air modeling, L.A.P. conducted the climate change analysis, M.M. prepared geospatial data for the i-Tree Cool Air model, and M.E.R. helped develop our scenario of total tree loss. All authors contributed to reviewing and editing. All authors wrote and edited the final manuscript.

Competing interests

The authors declare no competing interests.

Additional information

Supplementary information The online version contains supplementary material available at https://doi.org/10.1038/s41467-026-71825-x.

Correspondence and requests for materials should be addressed to Robert I. McDonald or TC Chakraborty.

Peer review information *Nature Communications* thanks Kelsey N. Ellis and the other anonymous reviewer(s) for their contribution to the peer review of this work. A peer review file is available.